Computation, Properties, and Realizability of the Characteristic Immittance Matrices of Nonuniform Multiconductor Transmission Lines

José A. Brandão Faria, *Fellow, IEEE*, and Rodolfo Araneo, *Senior Member, IEEE*

***Abstract*—Power lines are longitudinally nonuniform, nonsymmetrical systems, where ordinary modal analysis, originally conceived for uniform multiconductor transmission lines (MTL), can be utilized only as a zeroth-order approximation. In this paper, we present an accurate analysis of nonuniform MTLs based on the frequency-domain transmission-matrix formalism for $2n$-port systems, where two unequal characteristic immittance matrices need to be defined, one for forward propagation and another for backward propagation. This paper, focused on the characteristic (or surge) immittance matrices, shows how they can be computed, describes their general properties, and reveals, for the first time, that in some cases they may not be physically realizable, meaning that a matched termination made of purely passive lumped components may not exist. The matrix theory developed in the paper is illustrated with simulation results concerning three-phase power line configurations where resonance phenomena take place at certain critical frequencies.**

***Index Terms*—Characteristic immittance matrices, eigenvalue problems, multiconductor transmission lines, nonuniform transmission lines, resonance phenomena, Riccati equations.**

I. Introduction

THE subject matter of nonuniform multiconductor transmission lines (MTL) is an important research subject with applications ranging from microwave systems to power systems. This paper is a new contribution to the latter area, with special focus on the computation, properties and realizability of the characteristic immittance matrices.

The subject of modal analysis, for uniform multiconductor transmission line-structures, is relatively simple and is well understood, [1], [2]. However, the analysis of nonuniform MTLs is much more elaborated and poses new difficulties. For example, in a uniform MTL with $n + 1$ conductors, the per unit length line parameters are constant, the eigenvalue problem to be solved is of dimension n, the number of independent modes is n, and a single $n \times n$ characteristic impedance matrix is needed. Contrarily, in a nonuniform MTL, constant line parameters do not exist, the eigenvalue problem is of dimension $2n$, the number of independent modes is $2n$, and two $n \times n$ characteristic impedance matrices are needed.

The analysis of wave propagation in nonuniform MTLs, based on eigenvalue problems, was initially developed by Wedepohl and Indulkar in 1974 [3]. From then on, the interest on the topic of nonuniform MTLs kept increasing until today, including theory, numerical methods, and applications, [4]–[20].

Overhead power lines are, by their nature, nonuniform systems. In fact, line conductors do not run parallel to the ground due to sag [11]; the soil is not a flat surface and its conductivity varies along the line length [7]; the shield wires are not continuously connected to the ground [7], [18], [19], and sometimes are even interrupted at some towers [19]; line transposition schemes make conductors interchange position periodically along the line [15], etc.

The contributions of this paper are on the one hand, the systematic presentation of the subject of nonuniform MTLs, distinguishing between symmetrical and nonsymmetrical MTLs and, on the other hand, the discussion, for the first time, of the problem of the physical realizability of the characteristic impedance matrices.

This paper is organized into seven sections, the first of which is introductory. Section II is dedicated to basic results on the transmission matrix of nonsymmetrical two-conductor transmission lines, showing the intrinsic difference between the characteristic immittances of forward and backward propagating waves. The general case of $2n$-port MTLs is systematized and discussed in Section III considering both symmetrical and nonsymmetrical situations. The properties of the characteristic immittance matrices are derived in Section IV from energy considerations. Application examples, focused on three-phase power line configurations are examined in Section V, illustrating the computation and properties of the characteristic immittances, for forward and backward propagation, where the key question of the realizability of matched line terminations is examined. At last, results are discussed in Section VI, and conclusions are outlined in Section VII.

Manuscript received July 1, 2017; revised September 17, 2017 and January 8, 2018; accepted February 10, 2018. Date of publication March 16, 2018; date of current version May 4, 2018. This work was supported in part by the Fundação para a Ciência e a Tecnologia (UID/EEA/50008/2013) and in part by the Instituto de Telecomunicações (Project PC226). Paper no. TPWRD-00866-2017. *(Corresponding author: Jose A. Brandão Faria.)*

J. A. Brandão Faria is with the Instituto de Telecomunicações, Instituto Superior Técnico, Universidade de Lisboa, Lisbon 1049-001, Portugal (e-mail: brandao.faria@ieee.org).

R. Araneo is with the Electrical Engineering Division of the Department of Astronautical, Electrical and Energy Engineering, University of Rome La Sapienza, Rome 18-00184, Italy (e-mail: rodolfo.araneo@uniroma1.it).

Color versions of one or more of the figures in this paper are available online at http://ieeexplore.ieee.org.

Digital Object Identifier 10.1109/TPWRD.2018.2806491

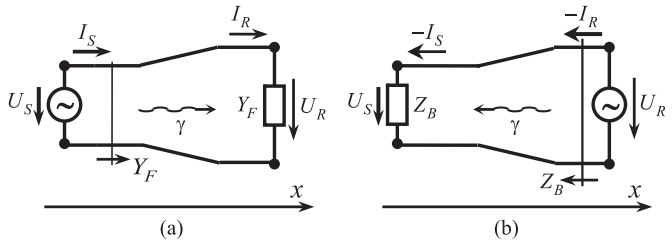

Fig. 1. Two-conductor nonuniform line. (a) Forward propagation along positive x. (b) Backward propagation along negative x.

II. Two-Conductor Transmission Lines

This section provides the basic matrix results for the analysis of nonuniform two-conductor transmission lines (TLs), useful for the analysis of the general case of MTL systems. The physical TL of length l is a two-port reciprocal network characterized in the frequency-domain by a transmission matrix T such that:

$$\begin{bmatrix} U_S \\ I_S \end{bmatrix} = \overbrace{\begin{bmatrix} a & b \\ c & d \end{bmatrix}}^{\mathbf{T}} \begin{bmatrix} U_R \\ I_R \end{bmatrix},$$

$$\begin{bmatrix} U_R \\ I_R \end{bmatrix} = \overbrace{\begin{bmatrix} d & -b \\ -c & a \end{bmatrix}}^{\mathbf{T}^{-1}} \begin{bmatrix} U_S \\ I_S \end{bmatrix}, \det\mathbf{T} = 1 \tag{1}$$

where U and I are voltage and current phasors, using the $\exp(j\omega t)$ option, and subscripts S and R are remainders for sending and receiving ends, respectively.

The diagonalization of matrix $\mathbf{T}$

$$\mathbf{M}^{-1}\mathbf{T}\mathbf{M} = \begin{bmatrix} \lambda_F & \\ & \lambda_B \end{bmatrix}, \mathbf{M} = [\mathbf{m}_F\ \mathbf{m}_B] = \begin{bmatrix} m_{11} & m_{12} \\ m_{21} & m_{22} \end{bmatrix} \tag{2}$$

produces a pair of complex eigenvalues λ_F and λ_B, such that

$$\begin{cases} \lambda_F + \lambda_B = a + d = \text{trace } \mathbf{T} \\ \lambda_F\lambda_B = 1 = \det \mathbf{T} \end{cases} \rightarrow \begin{cases} \lambda_F = e^{+\gamma l} \\ \lambda_B = e^{-\gamma l} \end{cases} \tag{3}$$

where γ is the propagation constant ($\gamma = \alpha + j\beta$, with α the attenuation constant, and β the phase constant).

The solution with $|\lambda_F| > 1$ refers to the *F*orward propagating wave, while the solution with $|\lambda_B| < 1$ refers to the *B*ackward propagating wave. The eigenvectors $\mathbf{m}_F$ and $\mathbf{m}_B$ associated with the above eigenvalues are determined through

$$\begin{bmatrix} a-\lambda_F & b \\ c & d-\lambda_F \end{bmatrix} \underbrace{\begin{bmatrix} m_{11} \\ m_{21} \end{bmatrix}}_{\mathbf{m}_F} = \begin{bmatrix} 0 \\ 0 \end{bmatrix} \tag{4a}$$

$$\begin{bmatrix} a-\lambda_B & b \\ c & d-\lambda_B \end{bmatrix} \underbrace{\begin{bmatrix} m_{12} \\ m_{22} \end{bmatrix}}_{\mathbf{m}_B} = \begin{bmatrix} 0 \\ 0 \end{bmatrix} \tag{4b}$$

Physical interpretation: For the **forward wave** [as shown in Fig. 1(a)] we have

$$\begin{cases} \frac{I_S}{U_S} = \frac{I_R}{U_R} = Y_F = Z_F^{-1} \\ \frac{U_S}{U_R} = \frac{I_S}{I_R} = \lambda_F = e^{+\gamma l} \end{cases} \tag{5}$$

where Y_F and Z_F denote the characteristic immittances of the forward wave. Plugging (5) into (1) leads to

$$\begin{cases} \begin{bmatrix} 1 \\ Y_F \end{bmatrix} U_S = \lambda_F \begin{bmatrix} 1 \\ Y_F \end{bmatrix} U_R = \begin{bmatrix} a\ b \\ c\ d \end{bmatrix} \begin{bmatrix} 1 \\ Y_F \end{bmatrix} U_R \\ \begin{bmatrix} a-\lambda_F & b \\ c & d-\lambda_F \end{bmatrix} \begin{bmatrix} 1 \\ Y_F \end{bmatrix} = \begin{bmatrix} 0 \\ 0 \end{bmatrix} \end{cases} \tag{6}$$

Comparing with (4a) we see that

$$\mathbf{m}_F = \begin{bmatrix} m_{11} \\ m_{21} \end{bmatrix} = \begin{bmatrix} 1 \\ Y_F \end{bmatrix} \rightarrow Y_F = m_{21}m_{11}^{-1} \tag{7}$$

For the **backward wave** [as shown in Fig. 1(b)] we have

$$\begin{cases} \frac{U_S}{-I_S} = \frac{U_R}{-I_R} = Z_B = Y_B^{-1} \\ \frac{U_S}{U_R} = \frac{I_S}{I_R} = \lambda_B = e^{-\gamma l} \end{cases} \tag{8}$$

where Z_B and Y_B denote the characteristic immittances of the backward wave. Plugging (8) into (1) leads to:

$$\begin{cases} \begin{bmatrix} -Z_B \\ 1 \end{bmatrix} I_S = \lambda_B \begin{bmatrix} -Z_B \\ 1 \end{bmatrix} I_R = \begin{bmatrix} a\ b \\ c\ d \end{bmatrix} \begin{bmatrix} -Z_B \\ 1 \end{bmatrix} I_R \\ \begin{bmatrix} a-\lambda_B & b \\ c & d-\lambda_B \end{bmatrix} \begin{bmatrix} -Z_B \\ 1 \end{bmatrix} = \begin{bmatrix} 0 \\ 0 \end{bmatrix} \end{cases} \tag{9}$$

Comparing with (4b) we see that

$$\mathbf{m}_B = \begin{bmatrix} m_{12} \\ m_{22} \end{bmatrix} = \begin{bmatrix} -Z_B \\ 1 \end{bmatrix} \rightarrow Z_B = -m_{12}m_{22}^{-1} \tag{10}$$

In conclusion, from (6)–(7) and (9)–(10), the $\mathbf{M}$ matrix of eigenvectors, in (2), can be put in the simple form:

$$\mathbf{M} = \begin{bmatrix} 1 & -Z_B \\ +Y_F & 1 \end{bmatrix} \tag{11}$$

III. Multiconductor Transmission Lines

Nonuniform MTLs can be split into two categories: symmetrical and nonsymmetrical. In a symmetrical MTL the sending and receiving ports are indiscernible, meaning that the ports can swap their designation without any effect; contrarily, in a nonsymmetrical MTL, the terminal ports are discernible.

A. Nonuniform Symmetrical MTLs

A nonuniform MTL is symmetrical when the MTL system is made of two identical nonuniform halves chain connected back to back. Note that the word symmetry is not related to any kind of lateral symmetry of the system, but instead, to longitudinal symmetry.

A symmetrical multiconductor transmission line of length l can be interpreted as a 2*n*-port reciprocal symmetric network

whose $2n \times 2n$ transmission matrix $\mathbf{T}$ is, [21], [22],

$$\begin{bmatrix} \mathbf{U}_S \\ \mathbf{I}_S \end{bmatrix} = \overbrace{\begin{bmatrix} \mathbf{A} & \mathbf{B} \\ \mathbf{C} & \mathbf{D} \end{bmatrix}}^{\mathbf{T}} \begin{bmatrix} \mathbf{U}_R \\ \mathbf{I}_R \end{bmatrix},$$

$$\begin{bmatrix} \mathbf{U}_R \\ \mathbf{I}_R \end{bmatrix} = \overbrace{\begin{bmatrix} \mathbf{A} & -\mathbf{B} \\ -\mathbf{C} & \mathbf{D} \end{bmatrix}}^{\mathbf{T}^{-1}} \begin{bmatrix} \mathbf{U}_S \\ \mathbf{I}_S \end{bmatrix}, \det \mathbf{T} = 1 \tag{12}$$

where, the submatrices $\mathbf{A}$, $\mathbf{B}$, $\mathbf{C}$, and $\mathbf{D}$ obey the following properties [21], [22]:

$$\begin{cases} \mathbf{A} = \mathbf{D}^T, \mathbf{D} = \mathbf{A}^T \\ \mathbf{B} = \mathbf{B}^T, \mathbf{C} = \mathbf{C}^T \end{cases} \quad \begin{cases} \mathbf{AB} = \mathbf{BD}, \mathbf{DC} = \mathbf{CA} \\ \mathbf{A}^2 - \mathbf{BC} = \mathbf{D}^2 - \mathbf{CB} = \mathbf{1} \end{cases} \tag{13}$$

The diagonalization of matrix $\mathbf{T}$ in (12), corresponding to the generalization of the results in (2), (3), and (11), is described through

$$\mathbf{M}^{-1}\mathbf{T}\mathbf{M} = \begin{bmatrix} e^{+\boldsymbol{\gamma} l} & \\ & e^{-\boldsymbol{\gamma} l} \end{bmatrix}, \mathbf{M} = \begin{bmatrix} \mathbf{M}_{11} & -\mathbf{Z}_B\mathbf{M}_{22} \\ +\mathbf{Y}_F\mathbf{M}_{11} & \mathbf{M}_{22} \end{bmatrix} \tag{14}$$

Therefore, we have:

$$\overbrace{\begin{bmatrix} \mathbf{A} & \mathbf{B} \\ \mathbf{C} & \mathbf{A}^T \end{bmatrix}}^{\mathbf{T}} \mathbf{M} = \mathbf{M} \begin{bmatrix} e^{+\boldsymbol{\gamma} l} & \\ & e^{-\boldsymbol{\gamma} l} \end{bmatrix} \tag{15a}$$

$$\underbrace{\begin{bmatrix} \mathbf{A} & -\mathbf{B} \\ -\mathbf{C} & \mathbf{A}^T \end{bmatrix}}_{\mathbf{T}^{-1}} \mathbf{M} = \mathbf{M} \begin{bmatrix} e^{-\boldsymbol{\gamma} l} & \\ & e^{+\boldsymbol{\gamma} l} \end{bmatrix} \tag{15b}$$

Summing and subtracting (15a) and (15b) yields:

$$\left(\frac{\mathbf{T} + \mathbf{T}^{-1}}{2}\right)\mathbf{M} = \begin{bmatrix} \mathbf{A} & \\ & \mathbf{A}^T \end{bmatrix} \mathbf{M} = \mathbf{M} \begin{bmatrix} \cosh \boldsymbol{\gamma} l & \\ & \cosh \boldsymbol{\gamma} l \end{bmatrix} \tag{16a}$$

$$\left(\frac{\mathbf{T} - \mathbf{T}^{-1}}{2}\right)\mathbf{M} = \begin{bmatrix} & \mathbf{B} \\ \mathbf{C} & \end{bmatrix} \mathbf{M} = \mathbf{M} \begin{bmatrix} \sinh \boldsymbol{\gamma} l & \\ & -\sinh \boldsymbol{\gamma} l \end{bmatrix} \tag{16b}$$

Substituting $\mathbf{M}$ into (16a) leads to

$$\begin{cases} \mathbf{M}_{11}^{-1}\mathbf{A}\mathbf{M}_{11} = \cosh \boldsymbol{\gamma} l \\ \mathbf{M}_{22}^{-1}\mathbf{A}^T\mathbf{M}_{22} = \cosh \boldsymbol{\gamma} l \end{cases} \rightarrow \quad \mathbf{M}_{22}^{-1} = \mathbf{M}_{11}^T \tag{17}$$

which permits the simultaneous calculation of $\mathbf{M}_{11}$, $\mathbf{M}_{22}$, and propagation constants $\boldsymbol{\gamma}$.

The symmetric characteristic immittance matrices $\mathbf{Z}_B$, $\mathbf{Z}_F$, $\mathbf{Y}_B$ and $\mathbf{Y}_F$ are determined by substituting $\mathbf{M}$ into (16b), yielding

$$\mathbf{M}_{11}^{-1} \begin{Bmatrix} \mathbf{B}\mathbf{Y}_F \\ \mathbf{Z}_F\mathbf{C} \end{Bmatrix} \mathbf{M}_{11} = \mathbf{M}_{22}^{-1} \begin{Bmatrix} \mathbf{Y}_B\mathbf{B} \\ \mathbf{C}\mathbf{Z}_B \end{Bmatrix} \mathbf{M}_{22} = \sinh \boldsymbol{\gamma} l \tag{18}$$

from where we learn that the forward and backward characteristic immittances coincide: $\mathbf{Z}_B = \mathbf{Z}_F = \mathbf{Z}_c$, $\mathbf{Y}_B = \mathbf{Y}_F = \mathbf{Y}_c$, their computation being possible through:

$$\begin{cases} \mathbf{Y}_c = \mathbf{B}^{-1}\mathbf{M}_{11}(\sinh \boldsymbol{\gamma} l)\mathbf{M}_{11}^{-1} \\ \mathbf{Z}_c = \mathbf{M}_{11}(\sinh \boldsymbol{\gamma} l)\mathbf{M}_{11}^{-1}\ \mathbf{C}^{-1} \end{cases} \tag{19}$$

or

$$\begin{cases} \mathbf{Y}_c = \mathbf{B}^{-1}(\mathbf{BC})^{1/2} = \mathbf{C}(\mathbf{BC})^{-1/2} \\ \mathbf{Z}_c = (\mathbf{BC})^{1/2}\mathbf{C}^{-1} = (\mathbf{BC})^{-1/2}\mathbf{B} \end{cases} \tag{20}$$

The results in (20) are particularly appealing since they allow the calculation of the MTL characteristic immittances directly from the $\mathbf{B}$ and $\mathbf{C}$ matrices.

B. Nonuniform Nonsymmetrical MTLs

Nonsymmetrical MTLs are those where the sending and receiving ends can be discerned. They are characterized by a transmission matrix $\mathbf{T}$ such that, [21], [22],

$$\begin{bmatrix} \mathbf{U}_S \\ \mathbf{I}_S \end{bmatrix} = \overbrace{\begin{bmatrix} \mathbf{A} & \mathbf{B} \\ \mathbf{C} & \mathbf{D} \end{bmatrix}}^{\mathbf{T}} \begin{bmatrix} \mathbf{U}_R \\ \mathbf{I}_R \end{bmatrix},$$

$$\begin{bmatrix} \mathbf{U}_R \\ \mathbf{I}_R \end{bmatrix} = \overbrace{\begin{bmatrix} \mathbf{D}^T & -\mathbf{B}^T \\ -\mathbf{C}^T & \mathbf{A}^T \end{bmatrix}}^{\mathbf{T}^{-1}} \begin{bmatrix} \mathbf{U}_S \\ \mathbf{I}_S \end{bmatrix}, \det \mathbf{T} = \mathbf{1} \tag{21}$$

where, the submatrices $\mathbf{A}$, $\mathbf{B}$, $\mathbf{C}$, and $\mathbf{D}$ obey the following properties [21], [22]:

$$\begin{cases} \mathbf{A}\mathbf{B}^T = \mathbf{B}\mathbf{A}^T, \mathbf{B}^T\mathbf{D} = \mathbf{D}^T\mathbf{B} \\ \mathbf{D}\mathbf{C}^T = \mathbf{C}\mathbf{D}^T, \mathbf{C}^T\mathbf{A} = \mathbf{A}^T\mathbf{C} \\ \mathbf{A}\mathbf{D}^T - \mathbf{B}\mathbf{C}^T = \mathbf{D}^T\mathbf{A} - \mathbf{B}^T\mathbf{C} = \mathbf{1} \end{cases} \tag{22}$$

The diagonalization of matrix $\mathbf{T}$ in (21), corresponding to the generalization of the results in (2), (3), and (11), is described through

$$\mathbf{T}\mathbf{M} = \mathbf{M} \begin{bmatrix} e^{+\boldsymbol{\gamma} l} & \\ & e^{-\boldsymbol{\gamma} l} \end{bmatrix}, \mathbf{M} = \begin{bmatrix} \mathbf{M}_{11} & -\mathbf{Z}_B\mathbf{M}_{22} \\ +\mathbf{Y}_F\mathbf{M}_{11} & \mathbf{M}_{22} \end{bmatrix} \tag{23}$$

To obtain $\mathbf{M}_{11}$, $\mathbf{M}_{22}$, $\mathbf{Z}_B$, $\mathbf{Y}_F$, and $e^{\pm\boldsymbol{\gamma} l}$ we tried the procedure exercised in (15)–(18) for symmetrical MTLs. Unfortunately, it does not work. None of the sought matrices can be obtained independently from reduced eigenvalue problems of order n. In fact, the analysis by block matrix partition of (23) produces:

$$\begin{cases} \mathbf{M}_{11}^{-1} \begin{Bmatrix} (\mathbf{A} + \mathbf{B}\mathbf{Y}_F) \\ \mathbf{Y}_F^{-1}(\mathbf{C} + \mathbf{D}\mathbf{Y}_F) \end{Bmatrix} \mathbf{M}_{11} = e^{+\boldsymbol{\gamma} l} \\ \mathbf{M}_{22}^{-1} \begin{Bmatrix} (\mathbf{D} - \mathbf{C}\mathbf{Z}_B) \\ \mathbf{Z}_B^{-1}(\mathbf{A}\mathbf{Z}_B - \mathbf{B}) \end{Bmatrix} \mathbf{M}_{22} = e^{-\boldsymbol{\gamma} l} \end{cases} \tag{24}$$

which has no obvious solutions.

The computation of $\mathbf{Y}_F$ and $\mathbf{Z}_B$ has been attempted in the literature [10], [18], [19] circumventing (23), considering instead:

$$\overbrace{\begin{bmatrix}\mathbf{U}_S\\ \mathbf{Y}_F\mathbf{U}_S\end{bmatrix}=\begin{bmatrix}\mathbf{A}&\mathbf{B}\\ \mathbf{C}&\mathbf{D}\end{bmatrix}\begin{bmatrix}\mathbf{U}_R\\ \mathbf{Y}_F\mathbf{U}_R\end{bmatrix}}^{\text{Forward Wave}},$$
$$\overbrace{\begin{bmatrix}-\mathbf{Z}_B\mathbf{I}_S\\ \mathbf{I}_S\end{bmatrix}=\begin{bmatrix}\mathbf{A}&\mathbf{B}\\ \mathbf{C}&\mathbf{D}\end{bmatrix}\begin{bmatrix}-\mathbf{Z}_B\mathbf{I}_R\\ \mathbf{I}_R\end{bmatrix}}^{\text{Backward Wave}} \tag{25}$$

which leads to

$$\begin{cases}\mathbf{C}-\mathbf{Y}_F\mathbf{A}+\mathbf{D}\mathbf{Y}_F-\mathbf{Y}_F\mathbf{B}\mathbf{Y}_F=\mathbf{0}\\ \mathbf{B}-\mathbf{A}\mathbf{Z}_B+\mathbf{Z}_B\mathbf{D}-\mathbf{Z}_B\mathbf{C}\mathbf{Z}_B=\mathbf{0}\end{cases} \tag{26}$$

The results in (26) define nonsymmetric algebraic Riccati equations (NARE) involving quadratic terms [23]–[25], whose numerical solution is neither simple nor easy to obtain. In addition, they give rise to a countless number of solutions. The sought NARE solutions for the characteristic immittance matrices in (26) are calculated using iterative techniques, [19]; among the obtained multiple solutions those lacking physical consistency must be excluded, hoping that only one survives. Assuming that the correct NARE solutions for $\mathbf{Y}_F$ and $\mathbf{Z}_B$ are found from (26), then, we can plug them into (24) and determine $\mathbf{M}_{11}$, $\mathbf{M}_{22}$, and $\exp(\pm\boldsymbol{\gamma}l)$.

At this stage, let us go back to the unsolved eigenvalue problems in (24). The pair of equations for $\mathbf{Y}_F$ in (24) is equivalent to:

$$\begin{aligned}&\mathbf{A}+\mathbf{B}\mathbf{Y}_F=\mathbf{Y}_F^{-1}(\mathbf{C}+\mathbf{D}\mathbf{Y}_F)\rightarrow\\ &\quad\rightarrow\mathbf{C}-\mathbf{Y}_F\mathbf{A}+\mathbf{D}\mathbf{Y}_F-\mathbf{Y}_F\mathbf{B}\mathbf{Y}_F=\mathbf{0}\end{aligned} \tag{27}$$

Also, the pair of equations for $\mathbf{Z}_B$ in (24) is equivalent to:

$$\begin{aligned}&\mathbf{D}-\mathbf{C}\mathbf{Z}_B=\mathbf{Z}_B^{-1}(\mathbf{A}\mathbf{Z}_B-\mathbf{B})\rightarrow\\ &\quad\rightarrow\mathbf{B}-\mathbf{A}\mathbf{Z}_B+\mathbf{Z}_B\mathbf{D}-\mathbf{Z}_B\mathbf{C}\mathbf{Z}_B=\mathbf{0}\end{aligned} \tag{28}$$

but the results in (27) and (28) are just a repetition of the NARE in (26).

In conclusion: For nonsymmetrical MTLs, one cannot compute the propagation constants and characteristic immittance matrices from reduced *n*th-order eigenvalue problems; we have to solve the complete eigenvalue problem of order 2*n*:

$$\mathbf{M}^{-1}\begin{bmatrix}\mathbf{A}&\mathbf{B}\\ \mathbf{C}&\mathbf{D}\end{bmatrix}\mathbf{M}=\begin{bmatrix}e^{+\boldsymbol{\gamma}l}&\\ &e^{-\boldsymbol{\gamma}l}\end{bmatrix},\mathbf{M}=\begin{bmatrix}\mathbf{M}_{11}&\mathbf{M}_{12}\\ \mathbf{M}_{21}&\mathbf{M}_{22}\end{bmatrix} \tag{29}$$

obtaining $\mathbf{Z}_B$ and $\mathbf{Y}_F$ through

$$\mathbf{Z}_B=-\mathbf{M}_{12}\mathbf{M}_{22}^{-1}=\mathbf{Y}_B^{-1}\,,\ \mathbf{Y}_F=+\mathbf{M}_{21}\mathbf{M}_{11}^{-1}=\mathbf{Z}_F^{-1} \tag{30}$$

which is a generalization of the particular results in (7) and (10) for the simple case of nonsymmetrical two-port networks ($n=1$) addressed in Section II.

The NARE approach (25)–(26) and the eigenvalue problems in (24) are distinct but equivalent methods; one leads to the other and vice-versa.

Contrarily to the case of symmetrical MTLs —see (20), it is not possible to analytically express $\mathbf{Z}_B$ and $\mathbf{Y}_F$ in terms of the **A**, **B**, **C** and **D** submatrices.

IV. Properties of the Characteristic Immittances

We start by showing the uniqueness property of the characteristic immittance matrices $\mathbf{Z}_B$ and $\mathbf{Y}_F$. The results in (29)–(30) involve a transformation matrix $\mathbf{M}$ that is not uniquely defined. Consider a different transformation $\tilde{\mathbf{M}}=\mathbf{M}\mathbf{N}$, where $\mathbf{N}$ is an arbitrary non-singular diagonal normalization matrix,

$$\begin{aligned}\tilde{\mathbf{M}}&=\begin{bmatrix}\tilde{\mathbf{M}}_{11}&\tilde{\mathbf{M}}_{12}\\ \tilde{\mathbf{M}}_{21}&\tilde{\mathbf{M}}_{22}\end{bmatrix}=\mathbf{M}\mathbf{N}\\ &=\begin{bmatrix}\mathbf{M}_{11}&\mathbf{M}_{12}\\ \mathbf{M}_{21}&\mathbf{M}_{22}\end{bmatrix}\begin{bmatrix}\mathbf{N}_1&\\ &\mathbf{N}_2\end{bmatrix}=\begin{bmatrix}\mathbf{M}_{11}\mathbf{N}_1&\mathbf{M}_{12}\mathbf{N}_2\\ \mathbf{M}_{21}\mathbf{N}_1&\mathbf{M}_{22}\mathbf{N}_2\end{bmatrix}\end{aligned} \tag{31}$$

If $\tilde{\mathbf{M}}$ replaces $\mathbf{M}$ in (29), then, knowing that diagonal matrices commute, we will still get

$$\tilde{\mathbf{M}}^{-1}\begin{bmatrix}\mathbf{A}&\mathbf{B}\\ \mathbf{C}&\mathbf{D}\end{bmatrix}\tilde{\mathbf{M}}=\begin{bmatrix}e^{+\boldsymbol{\gamma}l}&\\ &e^{-\boldsymbol{\gamma}l}\end{bmatrix} \tag{32}$$

Therefore, from (30), we see that

$$\begin{cases}\tilde{\mathbf{Z}}_B=-\tilde{\mathbf{M}}_{12}\tilde{\mathbf{M}}_{22}^{-1}=-\mathbf{M}_{12}\mathbf{N}_2\mathbf{N}_2^{-1}\mathbf{M}_{22}^{-1}\\ \qquad=-\mathbf{M}_{12}\mathbf{M}_{22}^{-1}=\mathbf{Z}_B\\ \tilde{\mathbf{Y}}_F=+\tilde{\mathbf{M}}_{21}\tilde{\mathbf{M}}_{11}^{-1}=+\mathbf{M}_{21}\mathbf{N}_1\mathbf{N}_1^{-1}\mathbf{M}_{11}^{-1}\\ \qquad=+\mathbf{M}_{21}\mathbf{M}_{11}^{-1}=\mathbf{Y}_F\end{cases} \tag{33}$$

proving the uniqueness of $\mathbf{Z}_B$ and $\mathbf{Y}_F$.

In Section V, dedicated to numerical simulations, we opted to normalize the $\mathbf{M}$ matrix such that in each and every column of $\mathbf{M}_{12}$ and $\mathbf{M}_{22}$ the entry with the largest absolute value is made equal to unity. This option permits the MTL currents to be comparable (the largest current is always made equal to 1 ampere for all the propagation modes).

Next, for the sake of brevity, we consider the case of forward propagation along a nonsymmetrical MTL driven at the sending port and terminated at the receiving port. The analysis of the reverse case of backward propagation is omitted, because it leads exactly to the same properties of the immittance matrix.

When an MTL is loaded with a network of lumped components mimicking the condition $\mathbf{U}_R=\mathbf{Z}_F\mathbf{I}_R$, reflection phenomena at the receiving end will not occur; all of the forward travelling wave energy will be absorbed by the termination. For sinusoidal regimes (frequency ω) the instantaneous power $p_R\,(t)$ at the receiving port is expressed as

$$p_R(t)=\sum_{k=1}^{n}u_{R_k}\,i_{R_k}=\underbrace{\Re\left[\frac{1}{2}\mathbf{I}_R^{*}\mathbf{U}_R\right]}_{P_a}+\underbrace{\Re\left[\frac{1}{2}\mathbf{I}_R^{T}\mathbf{U}_R\,e^{j2\omega t}\right]}_{p_o(t)} \tag{34}$$

where the symbol $*$ denotes conjugate transposed, P_a is the time-independent active power (i.e., the time-average of p_R),

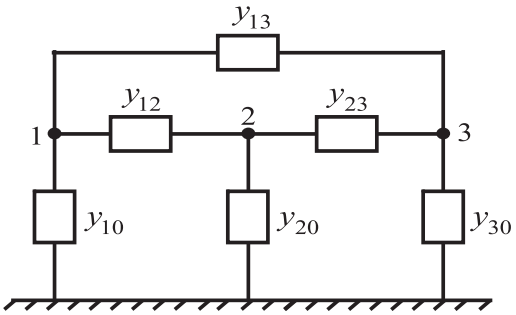

Fig. 2. Array of lumped admittances materializing a matched line termination.

and $p_o\,(t)$ is the sinusoidal oscillating power component of frequency 2ω. For an MTL terminated at the receiving port by $\mathbf{Z}_F$, the complex scalar term $\mathbf{I}_R^T\mathbf{U}_R$ is determined as:

$$\mathbf{I}_R^T\mathbf{U}_R = (\mathbf{I}_R^T\mathbf{U}_R)^T = \begin{cases} \mathbf{I}_R^T\mathbf{Z}_F\mathbf{I}_R \\ \mathbf{I}_R^T\mathbf{Z}_F^T\mathbf{I}_R \end{cases} \tag{35}$$

from where one gets $\mathbf{I}_R^T(\mathbf{Z}_F - \mathbf{Z}_F^T)\mathbf{I}_R = 0$, which allows two mathematical solutions. One solution is obvious: $\mathbf{Z}_F = \mathbf{Z}_F^T$, meaning that the $n \times n$ matrix $\mathbf{Z}_F$ must be symmetric. The other solution is $\mathbf{Z}_F$ equal to a skew-symmetric matrix (with zeroes along the main diagonal). However, the latter makes no sense, because if it hold true, then all two-conductor TLs ($n = 1$) would be characterized by $Z_F = 0$, which is absurd. Of course, the symmetry property of matrix $\mathbf{Z}_F$ is no novelty; we could have simply invoked the fact that the MTL is a reciprocal network.

Now, let us pay attention to the first term on the right hand side of (34). If at least one of the currents (or voltages) is not zero then the active power P_a delivered to the receiving load $\mathbf{Z}_F = \mathbf{R}_F + j\mathbf{X}_F$ will always be positive, that is:

$$2P_a = \Re\,[\mathbf{I}_R^*\mathbf{U}_R] = \mathbf{I}_R^*\mathbf{R}_F\mathbf{I}_R > 0 \tag{36}$$

or, similarly, using the load admittance $\mathbf{Y}_F = \mathbf{G}_F + j\mathbf{S}_F$,

$$2P_a = \Re\,[\mathbf{U}_\mathbf{R}^*\mathbf{I}_R] = \mathbf{U}_R^*\mathbf{G}_F\mathbf{U}_R > 0 \tag{37}$$

The positiveness of the quadratic Hermitian forms in (36)–(37) requires that the square symmetric real matrices $\mathbf{R}_F$ and $\mathbf{G}_F$ be positive definite. Its diagonal elements must all be positive as well as all its principal minors. For example, for $n = 3$:

$$\begin{cases} R_{F11} > 0, R_{F22} > 0, R_{F11}R_{F22} - R_{F12}^2 > 0, \\ \det\mathbf{R}_F > 0 \\ G_{F11} > 0, G_{F22} > 0, G_{F11}G_{F22} - G_{F12}^2 > 0, \\ \det\mathbf{G}_F > 0 \end{cases} \tag{38}$$

Note, however, that (38) does not enforce a positive or a negative value for the off-diagonal entries of $\mathbf{R}_F$ or $\mathbf{G}_F$.

At this point, it is important to clarify what is exactly the meaning of terminating the line with its characteristic immittance matrix; what kind of network made of lumped parameters is required at the MTL port to assure matching conditions (absence of reflected waves). Take the example in Fig. 2 illustrating the case of a three-phase line ($n = 3$), where the phase terminals

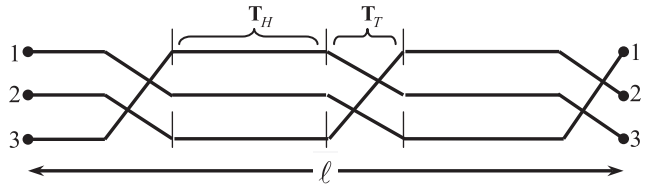

Fig. 3. Discretely transposed three-phase power line of total length l made of 3 uniform line sections of length l_1, l_2 and l_3, equal if the structure is periodic.

at the receiving port are interconnected by an array of lumped admittances $y_{ki} = g_{ki} + js_{ki}$.

On the one hand, by applying KCL at node k (for $k = 1, 2, 3$), we have

$$I_{k_R} = y_{k0}\,U_{k_R} + \sum_{i=1\,,\,i\neq k}^{n} y_{ki}(U_{k_R} - U_{i_R}) \tag{39}$$

On the other hand, from $\mathbf{I}_R = \mathbf{Y}_F\,\mathbf{U}_R$, we have

$$I_{k_R} = \sum_{i=1}^{n} Y_{F_{ki}}U_{i_R} \tag{40}$$

Comparing (39) and (40) leads to

$$\begin{cases} y_{k0} = g_{k0} + js_{k0} = \sum_{i=1}^{n} Y_{F_{ki}} \\ y_{ki} = g_{ki} + js_{ki} = -Y_{F_{ki}},\ i \neq k,\ i \neq 0 \end{cases} \tag{41}$$

V. Application Examples

In order to provide numerical evidence that negative conductances may be necessary for nonuniform MTL load matching we present, in this Section, two application examples of interest to the PES community. The first is concerned with the problem of discretely transposed three-phase lines, which we will examine in great detail. The second application, used as a confirmation, is concerned with the problem of three-phase lines with shield wires, where the latter are sectionalized (interrupted) or grounded along the line length.

A. Transposition

1) Transposed Three-Phase Line: For the purpose of mitigating line unbalancing, many overhead transmission lines have their conductors periodically transposed at discrete locations along the line length, [15]; a full transposition cycle comprising three cascaded line sections differing on the conductors sequence order. Because of local transpositions (see Fig. 3) the MTL structure is nonsymmetrical, ports S and R being discernible.

An analysis of such a structure has been conducted in [15], where horizontal, vertical, and triangular three-phase line configurations were considered; especial attention being paid to the resonance effects manifested in the frequency behavior of the MTL propagation constants (attenuation and phase velocity). In this paper we retake the subject, focusing on the horizontal configuration, using it to illustrate the computation and properties of the forward and backward characteristic immittance matrices – one aspect missing in [15].

As in [15], each section of the bilaterally symmetric horizontal MTL (modelled as a uniform system) is 100 km long, (i.e., $l_1 = l_2 = l_3 = 100$ km), is 10 m wide, and is placed 25 m above ground. The phase conductors have a dc resistance of 57.3 mΩ/km, and the soil resistivity is 100 Ωm. The overall line length is $l = l_1 + l_2 + l_3 = 300$ km, meaning that the first manifestation of resonance phenomena occurs at relative low frequencies, around 500 Hz, when $\beta l \simeq \pi$. Simulation results presented here consider the frequency window 450–550 Hz.

The global transmission matrix $\mathbf{T}$, of size 6×6, describing the MTL in Fig. 3, is

$$\mathbf{T} = \begin{bmatrix} \mathbf{A} & \mathbf{B} \\ \mathbf{C} & \mathbf{D} \end{bmatrix} = (\mathbf{T}_H \, \mathbf{T}_T)^3 \tag{42}$$

where $\mathbf{T}_H$ is the transmission matrix of a uniform horizontal line section, and $\mathbf{T}_T$ is the transmission matrix of the transposition segment:

$$\mathbf{T}_T = \begin{bmatrix} \mathbf{P} & \mathbf{0} \\ \mathbf{0} & \mathbf{P} \end{bmatrix}, \quad \mathbf{P} = \begin{bmatrix} 0 & 1 & 0 \\ 0 & 0 & 1 \\ 1 & 0 & 0 \end{bmatrix} \tag{43}$$

From the diagonalization of $\mathbf{T}$, we obtain

$$\mathbf{TM} = \mathbf{M} \begin{bmatrix} e^{+\boldsymbol{\gamma} l} & \\ & e^{-\boldsymbol{\gamma} l} \end{bmatrix}, \mathbf{M} = \begin{bmatrix} \mathbf{M}_{11} & \mathbf{M}_{12} \\ \mathbf{M}_{21} & \mathbf{M}_{22} \end{bmatrix} \tag{44}$$

yielding, from (30),

$$\begin{cases} \mathbf{Y}_B = \mathbf{Z}_B^{-1} = -\mathbf{M}_{22}\mathbf{M}_{12}^{-1} \\ \mathbf{Y}_F = \mathbf{Z}_F^{-1} = +\mathbf{M}_{21}\mathbf{M}_{11}^{-1} \end{cases} \tag{45}$$

At this point a crucial remark is necessary: When solving matrix eigenvalue problems, some commercial software packages produce a sequence of eigenvalues arbitrarily ordered. To correctly implement (44), the complex eigenvalues (as well as the corresponding eigenvectors) must be sorted appropriately. The first *n* eigenvalues λ_1, λ_2, λ_3, corresponding to forward propagation must be chosen such that $|\lambda_k| > 1$; the remaining eigenvalues, corresponding to backward propagation, must be reordered such that $\lambda_{k+n} = \lambda_k^{-1}$. Failing this step in (44)-(45) leads to characteristic immittance matrices erroneously calculated, with no meaning.

2) Simulation Results for a Fixed Frequency: Next we offer a sequence of numerical results computed at a single frequency (500 Hz), aimed to illustrate the characteristics of the forward and backward propagation modes, which, despite being different, share the same set of modal propagation constants:

$$\begin{cases} \gamma_1 = \alpha_1 + j\beta_1 \ , \ \text{with} \begin{cases} e^{-\alpha_1 l} = 0.9574 \\ \beta_1 l = 182.4^\circ \end{cases} \\ \gamma_2 = \alpha_2 + j\beta_2 \ , \ \text{with} \begin{cases} e^{-\alpha_2 l} = 0.8193 \\ \beta_2 l = 180.6^\circ \end{cases} \\ \gamma_3 = \alpha_3 + j\beta_3 \ , \ \text{with} \begin{cases} e^{-\alpha_3 l} = 0.7903 \\ \beta_3 l = 220.0^\circ \end{cases} \end{cases} \tag{46}$$

The difference between forward and backward modes is observed in the voltage and current distribution among conductors and also in the characteristic admittance matrices as shown in Table I.

Note that current and voltage values were computed by enforcing that the maximum conductor's current at the driving port is normalized to 1 ampere (see Section IV).

For any forward or backward propagating mode, the active powers computed at the sending and receiving ports are always positive, their ratio being related to mode attenuation through

$$\left(\frac{\frac{1}{2}\Re\left[\mathbf{I}_R^* \mathbf{U}_R\right]_{\text{mode } k}}{\frac{1}{2}\Re\left[\mathbf{I}_S^* \mathbf{U}_S\right]_{\text{mode } k}} \right)_F = \left(\frac{\frac{1}{2}\Re\left[-\mathbf{I}_S^* \mathbf{U}_S\right]_{\text{mode } k}}{\frac{1}{2}\Re\left[-\mathbf{I}_R^* \mathbf{U}_R\right]_{\text{mode } k}} \right)_B = e^{-2\alpha_k l} \tag{47}$$

Now we turn attention to the MTL characteristic immittance matrices. Firstly we note that the characteristic admittances $\mathbf{Y}_F$ and $\mathbf{Y}_B$ in Table I, although different, have some common entries: $Y_{F11} = Y_{B11}$, $Y_{F22} = Y_{B33}$, $Y_{F33} = Y_{B22}$, $Y_{F12} = Y_{B13}$, $Y_{F13} = Y_{B12}$, and $Y_{F23} = Y_{B23}$. This happens not only because the MTL is strictly periodic, but also because of the particular bilateral symmetry of the horizontal line configuration being used.

The results in Table I for $\mathbf{Y}_F$ and $\mathbf{Y}_B$ were checked for consistency: Matrices are symmetric. Their real parts are positive definite. They obey the NARE equations in (26).

Next, we computed the array of lumped parameters (see Fig. 2) that mimics the calculated characteristic immittance matrices, i.e., the parameters for matched termination.

A matched termination at port *R* requires the following phase-to-ground and inter-phase lumped admittances:

$$\begin{cases} y_{F10} = +1.507 - \text{j}0.062 \text{ mS} \\ y_{F20} = +0.605 + \text{j}0.273 \text{ mS} \\ y_{F30} = +1.263 - \text{j}0.038 \text{ mS} \end{cases},$$

$$\begin{cases} y_{F12} = +1.741 - \text{j}0.905 \text{ mS} \\ y_{F23} = +1.017 + \text{j}1.480 \text{ mS} \\ y_{F13} = -1.064 - \text{j}0.450 \text{ mS} \end{cases} \tag{48}$$

A matched termination at port *S* requires the following phase-to-ground and inter-phase lumped admittances:

$$\begin{cases} y_{B10} = +1.507 - \text{j}0.062 \text{ mS} \\ y_{B20} = +1.263 - \text{j}0.038 \text{ mS} \\ y_{B30} = +0.605 + \text{j}0.273 \text{ mS} \end{cases},$$

$$\begin{cases} y_{B12} = -1.064 - \text{j}0.450 \text{ mS} \\ y_{B23} = +1.017 + \text{j}1.480 \text{ mS} \\ y_{B13} = +1.741 - \text{j}0.905 \text{ mS} \end{cases} \tag{49}$$

Against ordinary expectation, we see from (48)–(49) that not all the lumped admittances have positive real part!

At port R a negative conductance exists between terminals 1 and 3; at port S a negative conductance exists between terminals

TABLE I
COMPUTED RESULTS FOR THE FORWARD AND BACKWARD MODES @ 500 HZ

Forward propagation modes (MTL driven at port S and matched at port R)		Backward propagation modes (MTL driven at port R and matched at port S)	
Mode 1 (aerial mode)			
$\overbrace{\begin{bmatrix} 0.998\angle -113.8^\circ \\ 0.964\angle +128.7^\circ \\ 1 \end{bmatrix}}^{\mathbf{I}_S}$ A $\underbrace{\begin{bmatrix} 0.955\angle +63.8^\circ \\ 0.923\angle -53.7^\circ \\ 0.957\angle +177.6^\circ \end{bmatrix}}_{\mathbf{I}_R}$ A	$\overbrace{\begin{bmatrix} 323.0\angle -118.6^\circ \\ 389.7\angle +117.5^\circ \\ 363.6\angle +13.9^\circ \end{bmatrix}}^{\mathbf{U}_S}$ V $\underbrace{\begin{bmatrix} 309.3\angle +59.0^\circ \\ 373.1\angle -64.9^\circ \\ 348.1\angle -168.5^\circ \end{bmatrix}}_{\mathbf{U}_R}$ V	$\overbrace{\begin{bmatrix} 0.998\angle -113.8^\circ \\ 1 \\ 0.964\angle +128.7^\circ \end{bmatrix}}^{\mathbf{I}_R}$ A $\underbrace{\begin{bmatrix} 0.955\angle +63.8^\circ \\ 0.957\angle +177.6^\circ \\ 0.923\angle -53.7^\circ \end{bmatrix}}_{\mathbf{I}_S}$ A	$\overbrace{\begin{bmatrix} 323.0\angle +61.4^\circ \\ 363.6\angle -166.1^\circ \\ 389.7\angle -62.5^\circ \end{bmatrix}}^{\mathbf{U}_R}$ V $\underbrace{\begin{bmatrix} 309.3\angle -121.0^\circ \\ 348.1\angle +11.5^\circ \\ 373.1\angle +115.1^\circ \end{bmatrix}}_{\mathbf{U}_S}$ V
Mode 2 (aerial mode)			
$\overbrace{\begin{bmatrix} 0.651\angle -171.6^\circ \\ 1 \\ 0.388\angle +166.2^\circ \end{bmatrix}}^{\mathbf{I}_S}$ A $\underbrace{\begin{bmatrix} 0.533\angle +7.8^\circ \\ 0.819\angle +179.4^\circ \\ 0.318\angle -14.4^\circ \end{bmatrix}}_{\mathbf{I}_R}$ A	$\overbrace{\begin{bmatrix} 282.4\angle -94.7^\circ \\ 63.9\angle -52.4^\circ \\ 348.8\angle +92.5^\circ \end{bmatrix}}^{\mathbf{U}_S}$ V $\underbrace{\begin{bmatrix} 231.4\angle +84.8^\circ \\ 52.4\angle +127.1^\circ \\ 285.8\angle -88.1^\circ \end{bmatrix}}_{\mathbf{U}_R}$ V	$\overbrace{\begin{bmatrix} 0.651\angle -171.6^\circ \\ 0.388\angle +166.2^\circ \\ 1 \end{bmatrix}}^{\mathbf{I}_R}$ A $\underbrace{\begin{bmatrix} 0.533\angle +7.8^\circ \\ 0.318\angle -14.4^\circ \\ 0.819\angle +179.4^\circ \end{bmatrix}}_{\mathbf{I}_S}$ A	$\overbrace{\begin{bmatrix} 282.4\angle +85.3^\circ \\ 348.8\angle -87.5^\circ \\ 63.9\angle +127.6^\circ \end{bmatrix}}^{\mathbf{U}_R}$ V $\underbrace{\begin{bmatrix} 231.4\angle -95.2^\circ \\ 285.8\angle +91.9^\circ \\ 52.4\angle -52.9^\circ \end{bmatrix}}_{\mathbf{U}_S}$ V
Mode 3 (ground mode)			
$\overbrace{\begin{bmatrix} 1 \\ 0.771\angle +2.3^\circ \\ 0.852\angle -8.9^\circ \end{bmatrix}}^{\mathbf{I}_S}$ A $\underbrace{\begin{bmatrix} 0.790\angle +140.0^\circ \\ 0.609\angle +142.3^\circ \\ 0.673\angle +131.1^\circ \end{bmatrix}}_{\mathbf{I}_R}$ A	$\overbrace{\begin{bmatrix} 733.1\angle -7.0^\circ \\ 820.0\angle -7.1^\circ \\ 794.1\angle -2.9^\circ \end{bmatrix}}^{\mathbf{U}_S}$ V $\underbrace{\begin{bmatrix} 579.4\angle +133.0^\circ \\ 648.1\angle +132.9^\circ \\ 627.6\angle +137.0^\circ \end{bmatrix}}_{\mathbf{U}_R}$ V	$\overbrace{\begin{bmatrix} 1 \\ 0.852\angle -8.9^\circ \\ 0.771\angle +2.3^\circ \end{bmatrix}}^{\mathbf{I}_R}$ A $\underbrace{\begin{bmatrix} 0.790\angle +140.0^\circ \\ 0.673\angle +131.1^\circ \\ 0.609\angle +142.3^\circ \end{bmatrix}}_{\mathbf{I}_S}$ A	$\overbrace{\begin{bmatrix} 733.1\angle +173.0^\circ \\ 794.1\angle +177.0^\circ \\ 820.0\angle +172.9^\circ \end{bmatrix}}^{\mathbf{U}_R}$ V $\underbrace{\begin{bmatrix} 579.4\angle -47.0^\circ \\ 627.6\angle -43.0^\circ \\ 648.1\angle -47.1^\circ \end{bmatrix}}_{\mathbf{U}_S}$ V
Characteristic admittance matrix $\mathbf{Y}_F$ (in mS):		Characteristic admittance matrix $\mathbf{Y}_B$ (in mS):	
$\begin{bmatrix} 2.184-j1.417 & -1.741+j0.905 & 1.064+j0.450 \\ -1.741+j0.905 & 3.363+j0.849 & -1.017-j1.480 \\ 1.064+j0.450 & -1.017-j1.480 & 1.215+j0.993 \end{bmatrix}$		$\begin{bmatrix} 2.184-j1.417 & 1.064+j0.450 & -1.741+j0.905 \\ 1.064+j0.450 & 1.215+j0.993 & -1.017-j1.480 \\ -1.741+j0.905 & -1.017-j1.480 & 3.363+j0.849 \end{bmatrix}$	

1 and 2. This is novel and reveals that it may not be possible to always find a matched termination for a nonuniform MTL using an array of purely passive lumped components.

3) Simulation Results for Variable Frequency: Now we let the frequency vary in the range 450–550 Hz.

The graphical plots in Fig. 4 are concerned with the frequency-dependent resonance features of the MTL propagation constants.

The subplot on the left shows the overall attenuation $\Re[\gamma_k(\omega)l]$ expressed in dB, for the three propagation modes ($k = 1, 2, 3$). The subplot on the right shows the normalized phase velocity$(\omega/\Im[\gamma_k])/v_0$, for the same modes, where v_0 is the light speed in free space. Mode 3, with the highest attenuation and smallest velocity is typical of a ground mode. Modes 1 and 2 are aerial modes, one of them showing abnormal sudden variations in the velocity and attenuation due to resonance effects caused by transposition. These results fully agree with those published in [15].

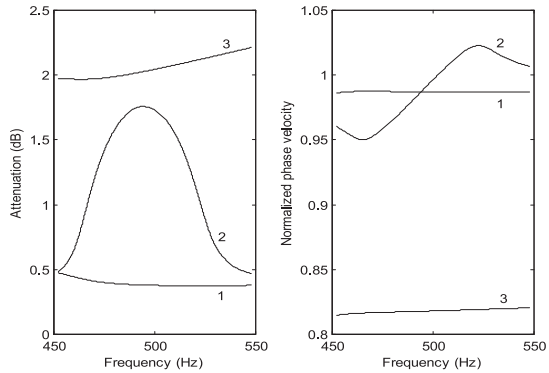

Fig. 4. Propagation constants (attenuation and normalized phase velocity) against frequency, for the aerial modes (1 and 2) and ground mode (3).

Next, we computed the lumped admittance parameters for matched load termination that mimic the calculated characteristic immittance matrices.

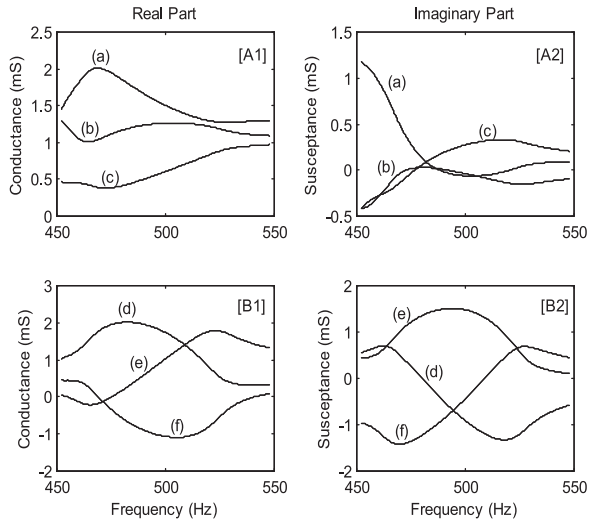

Fig. 5. Matching load admittance parameters. Subplots [A1] and [A2] on the top, refer to phase-to-ground conductances and susceptances, respectively. Subplots [B1] and [B2] on the bottom, refer to inter-phase conductances and susceptances, respectively. Curves (a) denote $y_{F\,10} = y_{B\,10}$. Curves (b) denote $y_{F\,30} = y_{B\,20}$. Curves (c) denote $y_{F\,20} = y_{B\,30}$. Curves (*d*) denote $y_{F\,12} = y_{B\,13}$. Curves (e) denote $y_{F\,23} = y_{B\,23}$. Curves (*f*) denote $y_{F\,13} = y_{B\,12}$.

Graphical plots against frequency of the real and imaginary parts of the phase-to-ground admittances y_{10}, y_{20}, y_{30}, and inter-phase admittances y_{12}, y_{13}, y_{23} were obtained, for both cases of forward and backward propagation.

Computed results for all the conductances and susceptances, plotted against frequency in the range 450–550 Hz, are shown in Fig. 5.

Again, we observe that curves (e) and (f) for the inter-phase conductances, shown in [B1], do exhibit negative values, contrarily to the phase-to-ground conductances in [A1] which are positive. Displayed susceptances change from inductive to capacitive, or vice versa, along the frequency range of analysis. We also obtained curves of the same parameters at lower frequencies (0–400 Hz) away from the center frequency of resonance, and in that case no negative conductances were found.

4) Simulation Results for Nonperiodic Transposition: The preceding simulations were obtained for a strictly periodic structure where $l_1 = l_2 = l_3 = 100$ km. Next we present more results considering usually shorter uniform line segments of length around 30 km with a full transposition cycle of total length $l = 90$ km, for which the first resonance frequencies occur at 1.7 kHz, 3.3 kHz and 5.0 kHz.

We observed the evolution of the 6 inter-phase matching conductances g_{ik} in the broad frequency range 1 to 5.5 kHz, considering increasingly severe deviations from the strictly periodic transposition scheme. Graphical plots of g_{ik}, presented in Fig. 6, were obtained for the following cases:

Case a) $l_1 = 26$ km, $l_2 = 28$ km, $l_3 = 36$ km
Case b) $l_1 = 36$ km, $l_2 = 21$ km, $l_3 = 33$ km
Case c) $l_1 = 22$ km, $l_2 = 42$ km, $l_3 = 26$ km

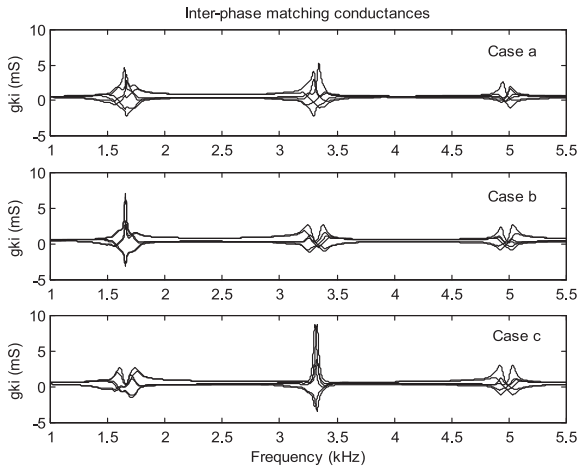

Fig. 6. Inter-phase matching conductances against frequency for the situation of nonperiodic transposition. The relative square mean value of the lengths deviations is 25% for case (a), 37% for case (b), and 50% for case (c).

The square mean value of the lengths deviations is 7.5 km for case a, 11.2 km for case b, and 15.0 km for case c.

The results in Fig. 6, confirm again that some of the six inter-phase conductances drop below zero near the resonance frequencies, no matter the magnitude of the lengths deviations.

B. Sectionalization

Overhead transmission lines have shield wires that are usually grounded at every tower for lightning protection purposes. Nevertheless, in some cases, shield wires are sectionalized (interrupted) at some towers for several reasons, mainly for reducing power losses [19]. These events destroy MTL uniformity, turning them into nonuniform structures.

Both practices have been studied separately; the effect of grounding in [7], [18], [26], and the effect of sectionalization in [27]. The combination of the two effects was analyzed in [19], [28], [29]. In all the cases, it was shown that detrimental consequences for PLC transmission may occur at resonance frequencies near 0.25 MHz (for a period of 600 m) or 0.5 MHz (for a period of 300 m). Fig. 7 shows schematically a general arrangement for grounding and sectionalization of a horizontal three-phase line with two shield wires; see details in [19]. For this configuration the frequency-dependence of the phase-to-ground matching conductance g_{10} was depicted in [19, Fig. 6] showing no negative values. Here, we complement that information by also presenting results for the inter-phase matching conductances g_{ik} , which, again, confirm the presence of negative values–see Fig. 8.

The results in Fig. 8, for g_{12}, g_{23}, and g_{13}, concern symmetrical periodic nonuniform structures of period 600 m, resonating near to 250 kHz. In this case, given the symmetry of the MTL, the forward and backward characteristic admittances coincide.

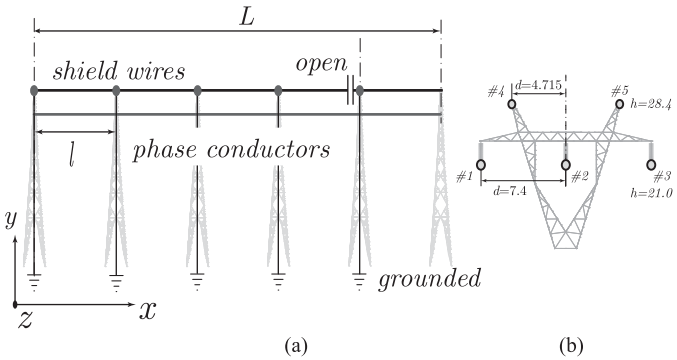

Fig. 7. Schematic representation of grounding and sectionalization (a) of a horizontal three-phase line with two shield wires (b). The dimensions shown in (b) are in meters.

VI. Discussion

Section V provided numerical evidence that matching a nonuniform MTL may need a load network with negative inter-phase conductances at both ports. We are aware that this never reported phenomenon is rather strange. Nonetheless, we are firmly convinced that the negative-conductance phenomenom is real and not caused by any sort of numerical noise. In fact: We considered two independent numerical applications, the transposed MTL in Section V-A, and the sectionalized MTL in Section V-B. The first application was run at University of Lisbon/Portugal, the second in University of Rome/Italy. We utilized different computers and different software tools. Both simulations provide the same evidence: the possibility of negative interwire surge conductances. Moreover, the computed surge immittance matrices obtained from the solution of the $2n$-order eigenvalue problem in (29)–(30) were checked and confirmed correct by direct substitution in the NARE equations in (26).

Of course, numerical evidence is not a formal proof. But, because of their complexity, the application examples offered in Section V are not amenable to a pure analytical approach that indisputably can prove the claim of negative interwire conductances. Meanwhile, the authors have analyzed a very simple nonuniform MTL geometry consisting of a lossless two-wire line parallel to ground, where the wires separation is not constant, and managed to prove, using only analytical means, that when the line length approaches one half wavelength, a negative interwire conductance is in fact unavoidable for load matching. These results, in the form of a companion paper, will soon be submitted for publication.

As referred to in (37) the active power P_a at the matched load can never be negative. For a simple MTL with $n = 2$, this means that the entries of the conductance matrix must be such that:

$$G_{11} > 0,\ G_{22} > 0,\ \ +\sqrt{G_{11}G_{22}} > G_m > -\sqrt{G_{11}G_{22}}$$

where, not violating any physical principle, G_m can be either positive or negative. Using a parallelism, we may remember that in a 2-windings transformer the stored magnetic energy is

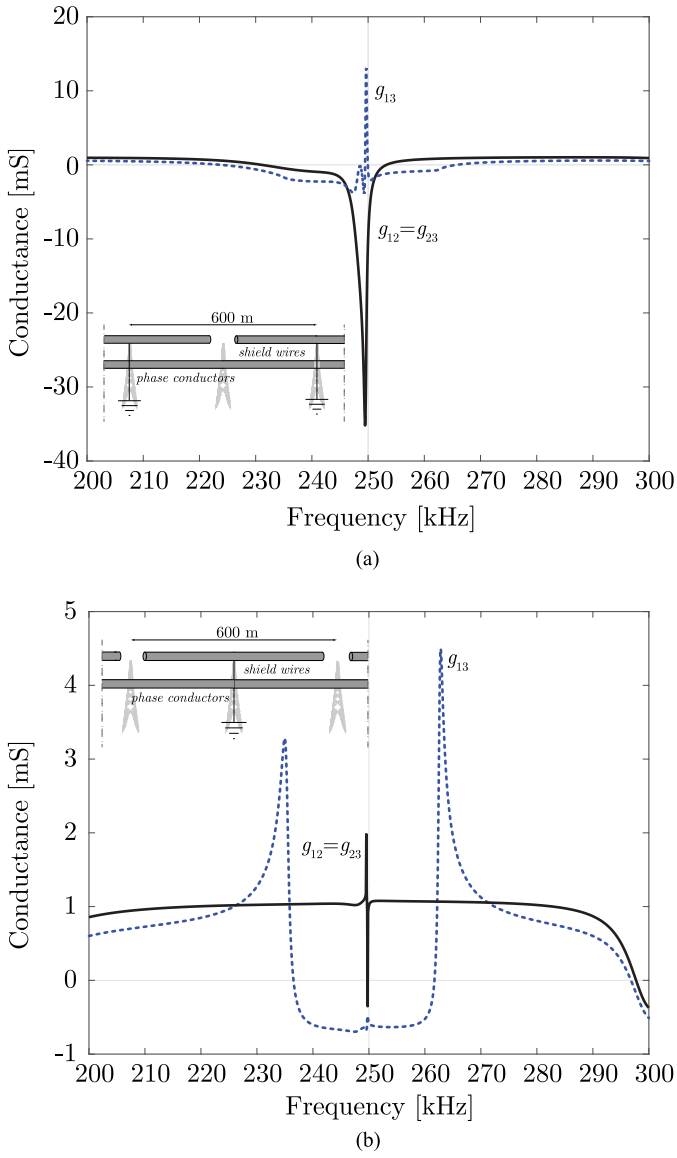

Fig. 8. Inter-phase matching conductances against frequency for the MTL configuration in Fig. 7, near the resonance frequency, for two different segmentation schemes. The curves in (a) refer to the case of shield wires grounded at the two ends of the MTL section and sectionalized at the middle tower. The curves in (b) refer to the case of shield wires sectionalized at the two ends of the MTL section and grounded at the middle tower.

given by

$$W_m = \tfrac{1}{2}L_1 i_1^2 + \tfrac{1}{2}L_2 i_2^2 + L_m i_1 i_2 > 0$$

where the positiveness of W_m is guaranteed no matter L_m is positive or negative.

The event of negative inter-phase matching conductances is surprising, unexpected and absolutely novel. But, it can only occur in nonuniform MTLs ($n > 1$), in a narrow frequency band, near halfwave resonance, when the length of the line approaches a multiple of $\lambda/2$ as evidenced in Section V. It cannot occur in uniform MTLs that do not resonate, and in two-conductor nonuniform lines ($n = 1$) where only one mode propagates.

Lastly: a word about the engineering implications of this work. There are no implications as far as the operation of power

lines is concerned, since power lines are not operated under load matching conditions. In addition, the standard power frequencies (50 or 60 Hz) will always be far away from typically higher resonance frequencies and, in that case, negative inter-phase matching conductances will not show up. In fact, for power frequencies and for power lines not very long, the utilization of wave propagation theory has no practical engineering implications, no matter the MTL is uniform or nonuniform. However, when dealing with power line transients or power line communications, things turn quite different; wave phenomena leading to high-frequency resonance effects cannot be ignored. These resonance effects are precisely linked with the surprising possibility of negative interwire surge conductances. Finally, we would like to stress that engineering is not only about practice, it is also about expanding knowledge. The never suspected event that nonuniform MTLs cannot always be matched by purely passive networks is an important new contribution to the field of MTLs at large.

VII. Conclusion

Using the frequency-domain transmission-matrix formalism, this article dwelt with $2n$-port nonuniform reciprocal multiconductor transmission line-systems, whose characterization requires, in general, two unequal characteristic wave immittance matrices, one for forward propagation and another for backward propagation. These matrices cannot be expressed directly in terms of the ABCD entries of the transmission matrix; their computation can be done using two methods, which were shown to be equivalent: solving a linear eigenvalue-eigenvector problem of dimension $2n$, or solving two nonlinear (quadratic) nonsymmetric Riccati matrix equations of dimension n.

The properties of the characteristic (or surge) immittance matrices: uniqueness, symmetry, and positive definiteness of their real parts, were derived employing physical principles. A revealed novelty is that matched line loads built from passive lumped components, mimicking the characteristic wave immittance matrices, may not always be realizable, since negative conductances may be needed near resonance frequencies. The theoretical aspects presented in the paper were illustrated with two MTL application examples of interest to the PES community: the first concerning the case of discretely transposed three-phase lines, the second concerning the case of three-phase lines with sectionalized shield wires.

References

[1] J. A. Brandao Faria, *Multiconductor Transmission-Line Structures—Modal Analysis Techniques*. Hoboken, NJ, USA: Wiley, 1993.

[2] C. R. Paul, *Analysis of Multiconductor Transmission Lines*. Hoboken, NJ, USA: Wiley, 2008.

[3] L. M. Wedepohl and C. S. Indulkar, "Wave propagation in nonhomogeneous systems. Properties of the chain matrix," *Proc. Inst. Elect. Eng.*, vol. 121, no. 9, pp. 997–1000, Sep. 1974.

[4] C. Menemenlis and Z. T. Chun, "Wave propagation on nonuniform lines," *IEEE Trans. Power. App. Syst.*, vol. PAS-101, no. 4, pp. 833–839, Apr. 1982.

[5] A. Ametani and M. Aoki, "Line parameters and transients of a non-parallel conductors systems," *IEEE Trans. Power Del.*, vol. 4, no. 2, pp. 1117–1126, Apr. 1989.

[6] M. M. Saied, A. S. AlFuhaid, and M. E. El-Shandwily, "s-Domain analysis of electromagnetic transients on nonuniform lines," *IEEE Trans. Power Del.*, vol. 5, no. 4, pp. 2072–2083, Oct. 1990.

[7] J. A. Brandão Faria, "On the resonance effects due to ground wires in transmission lines with non-uniform soil conductivity and non-uniform tower resistances," *IEEE Trans. Power Del.*, vol. 7, no. 1, pp. 29–38, Jan. 1992.

[8] M. T. C. de Barros and M. E. Almeida, "Computation of electromagnetic transients on nonuniform transmission lines," *IEEE Trans. Power Del.*, vol. 11, no. 2, pp. 1082–1091, Apr. 1996.

[9] A. AlFuhaid, E. Oufi, and M. Saied, "Application of nonuniform-line theory to the simulation of electromagnetic transients in power systems," *Int. J. Elect. Power Energy Syst.*, vol. 20, no. 3, pp. 225–233, 1998.

[10] J. Nitsch, "Exact analytical solution for nonuniform multiconductor transmission lines with the aid of the solution of a corresponding matrix Riccati equation," *Elect. Eng.*, vol. 81, no. 2, pp. 117–120, 1998.

[11] J. A. Brandão Faria, "High frequency modal analysis of lossy non-uniform three-phase overhead lines taking into account the catenary effect," *Eur. Trans. Elect. Power*, vol. 11, no. 3, pp. 195–201, 2001.

[12] J. A. Brandão Faria, "On the segmentation method used for analyzing nonuniform transmission lines: Application to the exponential line," *Eur. Trans. Elect. Power*, vol. 12, no. 5, pp. 361–368, 2002.

[13] A. Semlyen, "Some frequency domain aspects of wave propagation on nonuniform lines," *IEEE Trans. Power Del.*, vol. 18, no. 1, pp. 315–322, Jan. 2003.

[14] A. I. Ramirez, A. Semlyen, and R. Iravani, "Modeling nonuniform transmission lines for time domain simulation of electromagnetic transients," *IEEE Trans. Power Del.*, vol. 18, no. 3, pp. 968–974, Jul. 2003.

[15] J. A. Brandão Faria and M. G. das Neves, "Nonuniform three-phase power lines: Resonance effects due to conductor transposition," *Int. J. Elect. Power Energy Syst.*, vol. 26, no. 2, pp. 103–110, 2004.

[16] J. A. Brandão Faria, "A new generalized modal analysis theory for nonuniform multiconductor transmission lines," *IEEE Trans. Power Syst.*, vol. 19, no. 2, pp. 926–933, May 2004.

[17] J. A. Brandão Faria, "A new modal analysis theory for multiconductor nonuniform transmission-line structures: Application to the analysis of line junctions," *IEEE Trans. Power Syst.*, vol. 19, no. 3, pp. 1380–1386, Aug. 2004.

[18] A. Andreotti, D. Assante, and L. Verolino, "Characteristic impedance of periodically grounded lossless multiconductor transmission lines and time-domain equivalent representation," *IEEE Trans. Electromagn. Compat.*, vol. 56, no. 1, pp. 221–230, Feb. 2014.

[19] R. Araneo, J. A. Brandão Faria, and S. Celozzi, "Frequency-domain analysis of sectionalized shield wires on PLC transmission over high-voltage lines," *IEEE Trans. Electromagn. Compat.*, vol. 59, no. 3, pp. 853–861, Jun. 2017.

[20] K. K. M. A. Kariyawasam, S. Fan, A. M. Gole, and H. M. J. S. P. D. Silva, "Accurate validation of electromagnetic transient models of cascaded power transmission systems," in *Proc. IEEE Power Energy Soc. Gen. Meeting*, Jul. 2016, pp. 1–5.

[21] J. A. Brandão Faria, "Multimodal propagation in multiconductor transmission lines," *J. Electromagn. Waves Appl.*, vol. 28, no. 14, pp. 1677–1702, 2014.

[22] J. A. Brandão Faria, "On the transmission matrix of 2n-port reciprocal networks," *Microw. Opt. Technol. Lett.*, vol. 33, no. 3, pp. 151–154, 2002.

[23] H.-B. Meyer, "The matrix equation AZ + B - ZCZ - ZD = 0," *SIAM J. Appl. Math.*, vol. 30, no. 1, pp. 136–142, 1976.

[24] H.-B. Meyer, "Matrix Riccati solutions," *Linear Algebra Appl.*, vol. 20, no. 2, pp. 131–146, 1978.

[25] G. Freiling, "A survey of nonsymmetric Riccati equations," *Linear Algebra Appl.*, vol. 351, pp. 243–270, 2002.

[26] R. G. Olsen, "Propagation along overhead transmission lines with multiply grounded shield wires," *IEEE Trans. Power Del.*, vol. 32, no. 2, pp. 789–798, Apr. 2017.

[27] J. A. Brandão Faria, "Broadband resonance effects in power lines with sectionalized shield wires," in *Proc. IEEE Southeastcon*, Apr. 1990, vol. 2, pp. 654–658.

[28] S. Yang and G. Franklin, "Effects of segmented shield wires on signal attenuation of power-line carrier channels on overhead transmission lines—Part I: Modeling method," *IEEE Trans. Power Del.*, vol. 28, no. 1, pp. 427–433, Jan. 2013.

[29] S. Yang and G. Franklin, "Effects of segmented shield wires on signal attenuation of power-line carrier channels on overhead transmission lines—Part II: Signal attenuation results analysis," *IEEE Trans. Power Del.*, vol. 28, no. 1, pp. 434–441, Jan. 2013.